NEAR REAL TIME CONFOCAL MICROSCOPY OF CULTURED AMELANOTIC CELLS: SOURCES OF SIGNAL, CONTRAST AGENTS AND LIMITS OF CONTRAST

Colin Smithpeter, Andrew Dunn, Rebekah Drezek, Tom Collier, Rebecca Richards-Kortum

The University of Texas at Austin, Department of Electrical and Computer Engineering, Austin, Texas 78712

ABSTRACT

The use of high resolution, *in vivo* confocal imaging for noninvasive assessment of tissue pathology may offer a clinically important adjunct to standard histopathological techniques. To augment the present understanding of both the capabilities and limitations of *in vivo* confocal imaging, we investigated cellular sources of image contrast in amelanotic tissues, how contrast can be enhanced with external agents and how contrast is degraded by the scattering of overlying cells. A high-resolution reflected light confocal microscope was constructed and used to obtain images of various types of unstained amelanotic cells in suspension in real time before and after the addition of contrast agents. Reflectance images were compared to phase contrast images and electron micrographs to identify morphology visible with real time reflected light confocal microscopy. Mechanisms which decrease image contrast, including interference effects and scattering in overlying layers of cells, were considered. In amelanotic epithelial cells, fluctuations in the nuclear index of refraction provide signal which can be imaged even under several overlying cell layers. Acetic acid is an external contrast agent which can enhance this nuclear backscattering. Image contrast is degraded by the presence of multiple scattering in overlying cell layers. The degradation of image contrast by cell scattering depends on the scattering phase function; *in vitro* models which use polystyrene microspheres to approximate tissue underestimate the actual degradation caused by cell scattering. The loss in contrast can be explained using a finite difference time domain model of cellular scattering. We conclude that near real time reflected light confocal microscopy can be used to study cell morphology *in vivo*. Contrast degradation due to overlying tissue is a concern and cannot adequately be modeled using conventional tissue phantoms; however, acetic acid may be used to substantially increase intrinsic contrast, allowing imaging at significant depths despite distortion from overlying layers. © *1998 Society of Photo-Optical Instrumentation Engineers.* [S1083-3668(98)00804-1]

Keywords confocal microscopy; neoplasia; scattering; imaging; near real time.

1 INTRODUCTION

The use of high resolution, *in vivo* confocal imaging for noninvasive assessment of tissue pathology may offer a clinically important adjunct to standard histopathological techniques. Confocal microscopy obtains images in the superficial layers of tissue that are opaque to conventional microscopes by rejecting out of focus light.[1] Previous work has demonstrated the potential for *in vivo* confocal imaging in the superficial layers of the liver,[2] the transparent cornea,[2–4] and the epidermis,[5–8] where much of the confocal signal arises from backscattering of melanin. Prior studies[9] suggest that confocal imaging has the ability to image multiple cell layers in scattering amelanotic tissues as well. To augment the present understanding of both the capabilities and limitations of *in vivo* confocal imaging, it is important to investigate the cellular sources of image contrast and how contrast is degraded by the scattering of overlying cells.

The appearance of cells viewed confocally is highly dependent on cell morphological and biochemical structure. In recent images of skin,[7] it was shown that the cells containing melanin appeared to have bright cytoplasm and dark nuclei. Images were obtained through the epidermis and into the dermal papillae, up to 150 μm below the surface. The potential for *in vivo* pathology was demonstrated by the positive correlation between nuclear to cytoplasm (N/C) volume ratios measured by the confocal microscope and the N/C ratios measured

Colin Smithpeter, current address: Sandia National Laboratories, Albuquerque, NM 87185-0986.
Andrew Dunn, current address: Beckman Laser Institute and Medical Clinic, University of California, Irvine, Irvine, CA 92697-1875.
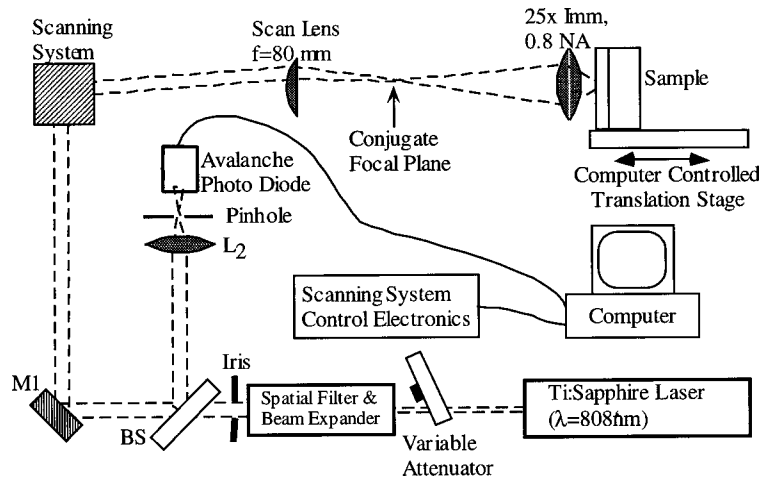
Fig. 1 Schematic of the confocal microscope built to acquire cellular images from reflected light.

in conventional histology of the imaged sites. In images of the corneal epithelium,[4] the appearance of the cells differed among layers. In the superficial epithelium, the nucleus had a reflective center region surrounded by a dark band and a reflective cytoplasm. In deeper layers, the dark band was not visible and the brightness of the cytoplasm was decreased. In the basal layer, the nuclear signal was faint compared to the reflections from the cell borders. Jester[2] imaged the superficial layers of several organs exposed by laparotomy in a rat. The hepatocytes in the liver appeared to have nuclei with bright centers, identified as nucleoli, and a surrounding dark band.

To accurately interpret confocal images, it is necessary to understand how contrast varies with tissue composition. Monte Carlo simulations[10] have demonstrated that fluctuations in refractive index are the largest source of contrast in confocal images of scattering tissue. However, the relationship between cell morphology and the refractive index profile is not well understood, and little experimental work has been completed to confirm Monte Carlo predictions.

This paper describes a study designed to (1) understand which features of epithelial cell morphology can be probed using near real time *in vivo* reflected light confocal microscopy, (2) understand how these features can be enhanced by application of exogenous contrast agents, and (3) understand how contrast in the images is degraded by the presence of such effects as interference and multiple scattering. We constructed a high-resolution reflected light confocal microscope to obtain images at 15 frames per second. We used this system to obtain images of various types of unstained amelanotic cells in suspension in real time before and after the addition of contrast agents. We compared these reflectance images to phase contrast images and electron micrographs to identify the features of cells visible with near real time reflected light con-

focal microscopy. In addition, mechanisms, which decrease image contrast, including interference effects and scattering in overlying layers of cells, are considered. A finite difference time domain (FDTD) model of cellular scattering is used to explain an observed loss of contrast. We conclude that near real time reflected light confocal microscopy can be used to study cell morphology *in vivo*; in amelanotic epithelial cells, fluctuations in the nuclear index of refraction provide signal which can be imaged even under several overlying cell layers. Acetic acid is an external contrast agent, which can enhance this nuclear backscattering. The degradation of image contrast by cell scattering depends on the scattering phase function, *in vitro* models which use polystyrene microspheres to approximate cell scattering underestimate the actual degradation caused by cell scattering.

2 METHODS

2.1 INSTRUMENTATION

A confocal microscope was constructed as shown in Figure 1. The microscope consisted of a laser, scanning system, intermediate optics, and a detector. Light from a Ti:sapphire laser ($\lambda = 808$ nm) was spatially filtered and recollimated to a diameter of 5 mm. A beam splitter transmitted 50% of the collimated light to a scanning system that deflected the laser light by angle in the x and y directions around the optical axis. The scanning system consisted of an 8 kHz resonant galvanometer and a 15 Hz galvanometer mounted at right angles (General Scanning VSH-8). A scan lens ($f = 80$ mm doublet) brought the light exiting the scanning system to a focus at the back focal plane of a 25× (Zeiss 461625, 0.8 NA, 160 mm) water immersion objective. The oscillations of the scan system mirrors scanned the laser light in a raster pattern at the focal plane of the objective lens. The light reflected backward

from the focal plane of the objective, within the NA of the objective, returned through the scanning system. A beamsplitter reflected half of the de-scanned light to lens L2 ($f=50.4$ mm). A 15 μm diameter pinhole at the focus of L2, a conjugate image plane, rejected light backscattered from outside the focal volume illuminated. The dimensionless pinhole radius corresponding to the L2 and 15 μm pinhole combination was 3, previously noted[11] as the radius for ideal confocal performance. An avalanche photodiode (APD) (Hamamatsu C5460) converted the light passing through the pinhole to a voltage. A PC video card sampled the APD voltage at intervals provided by the scan system electronics to construct images at a rate of 15 frames per second. The resulting image was a map of the reflectance values from the focal plane of the microscope. The user saved images of interest to a 512×512 pixel computer file with 256 gray levels. Alternatively, a super-VHS VCR recorded dynamic events. A computer-controlled translation stage with 1 μm resolution scanned samples through the focal plane.

The microscope's lateral resolution was quantified using a mirrored grating. The lateral resolution was defined as the distance to go from 90% to 10% of the signal at an edge transition from light to dark. The axial resolution was measured as the FWHM of the signal peak created by translating a mirror through the focus of the objective. To illustrate the lateral resolution, a grating with 3 μm line separation (300 lines/mm) and a group of 1 μm diameter polystyrene microspheres in contact with each other were imaged.

2.2 CELL AND TISSUE STUDIES

To determine the contrast available from cellular structure in human breast cancer cells, *in vitro* cell suspensions were imaged with the confocal microscope. The cell suspensions contained epithelial cells from the MCF-7 McGuire (early-stage malignancy) cell line. Before imaging, the cells were allowed to settle onto a layer of gelatin ($n=1.36$) to stabilize the image while minimizing the background signal from the supporting surface. No dyes or contrast agents were used. A comparison of the confocal images to images from a phase contrast microscope and electron micrographs of similar cells identified the cellular structure providing signal contrast.

Because optical interference effects had previously been reported as a problem in reflectance confocal imaging,[12,13] we imaged several different cell types with varying shape and size including human red blood cells and algae cells. The resulting confocal images were monitored for stability over time and for interference patterns such as fringes or speckle.

To investigate the effect of multiple scattering by overlying cell scattering on image contrast, images of cells were taken through multiple layers of cells.
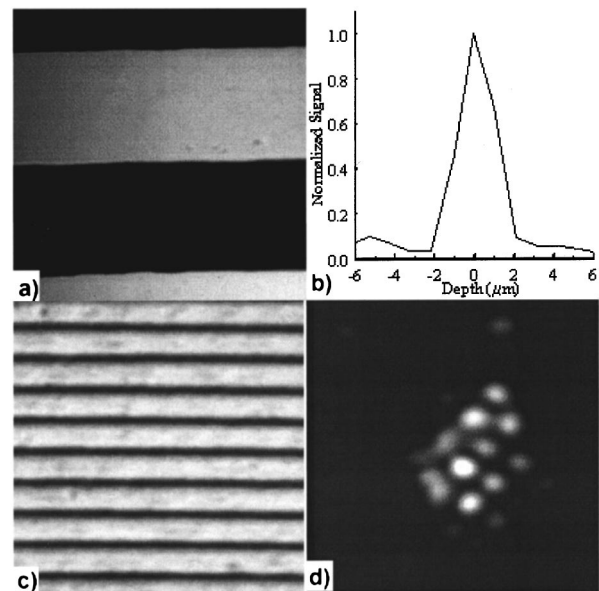

Fig. 2 (a) Confocal image of the 500 lines/in. grating in which each line is 25 μm wide. (b) Plot of intensity versus depth relative to the focal plane for a mirror translated through the focal plane. (c) Confocal image of a 300 lines/mm grating where each line is separated by 3.3 μm and (d) a cluster of 1 μm diameter polystyrene microspheres.

The layers were created by centrifuging the breast cancer cells into a pellet. Multiple images were acquired at different depths within the layers of cells in the pellet resting on a gelatin base. To explore the effects of the cell scattering on the microscope's lateral resolution, a 300 lines/mm mirrored grating was imaged under several layers of cells. The effect of overlying scattering on the axial resolution was quantified by measuring the FWHM of the signal peak from the index mismatch between the saline cell suspension and the underlying microscope slide.

Methods to improve image contrast were explored as well. Acetic acid is used for contrast enhancement in colposcopic inspection of the cervix. To assess the effect of acetic acid on the contrast in confocal imaging, breast cancer cells were imaged before and after exposure to 3% acetic acid. 5-aminolevulinic acid (ALA) is a clinically approved chromophore known to concentrate within neoplastic cells.[14] ALA was evaluated as a potential contrast agent by imaging the breast cancer cells before and after immersion in a 1% solution of ALA.

3 RESULTS

An average lateral resolution of 0.8 μm was measured from the image of a mirrored grating (500 lines/in.) shown in Figure 2(a). Figure 2(b) shows the signal peak created by translating a mirror through the focus of the objective peak; a FWHM axial resolution of 2 μm was measured from this signal. Figures 2(c) and 2(d) show images of a grat-
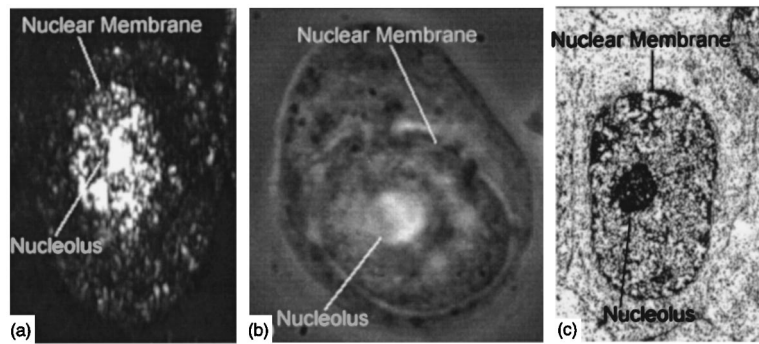
Fig. 3 (a) Confocal image of a breast cancer cell. (b) Phase contrast image of a breast cancer cell. (c) Electron micrograph of a breast cancer cell taken from Ref. 15.

ing with 3 μm line separation (300 lines/mm) and a group of 1 μm polystyrene spheres in contact with each other.

A confocal image of a breast cancer cell in suspension is shown in Figure 3(a) along with images from a phase contrast microscope [Figure 3(b)] and an electron micrograph [Figure 3(c)] taken from Ref. 15. Comparing these images reveals that the majority of the confocal signal is returned from the nucleolus and the clumps of chromatin material within the nucleus. The outline of the cell membrane is distinguished by the absence of signal rather than distinct signal from the membrane.

Although no optical interference effects were observed in the breast cancer cell images, distinct interference patterns were observed in images of other types of cells. Figure 4(a) shows an image of a red blood cell, with characteristic circular interference fringes. Figure 4(b) is a typical image of algae cells which display one or two fringes at the periphery of the cells.

To approximate tissue, images were acquired from a multilayer cell pellet of breast cancer cells at a number of depths. Figure 5 shows microscope images from a superficial layer [Figure 5(a)] and a layer 150 μm deep [Figure 5(b)]. In the superficial layer, it was possible to observe distinct structure within the nucleus and the outline of the cell. This particular image showed several distinct clusters of chromatin material within the nucleus. At a depth of 150 μm (approximately nine layers of cells), the contrast in the image was degraded as shown in Figure 5(b). Based upon the relative sizes, the bright areas are the nuclei and the signal in-between is from the cytoplasm. Although it was possible to distinguish individual nuclei, any detail about the structure within the nuclei was reduced. It was not possible to distinguish where one cell membrane began and another ended.

The observed loss of contrast might be explained by a loss of spatial resolution due to refraction of the light by the overlying cells. If so, this would differ from measurements of spatial resolution in tissue phantoms using suspensions of 1.0 μm diameter polystyrene microspheres which have a scattering coefficient and phase function similar to that of tissue. It has been reported[16] that lateral resolution is maintained through more than five optical depths of scattering from spheres. To compare the effects of cell scattering and polystyrene sphere scattering on lateral resolution, a 300 lines/mm grating was imaged under several layers of cells [Figure 6(a)] and a suspension of 1.0 μm diameter polystyrene spheres with a similar optical density
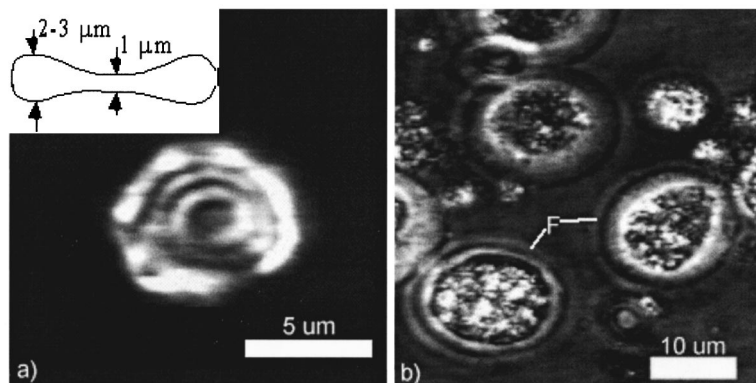

Fig. 4 (a) Confocal image of a red blood cell with (Inset) illustration of the typical red blood cell shape and dimensions. (b) Confocal image of algae cells with apparent (F) fringes.
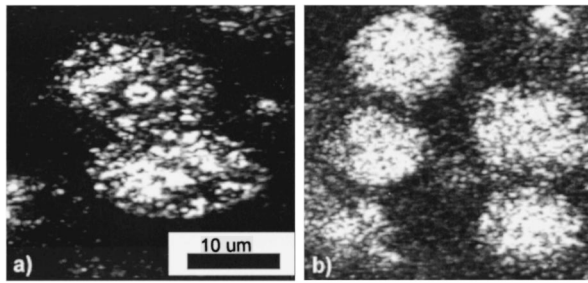
Fig. 5 Confocal image from (a) the superficial layer of cells and (b) a layer of cells 150 μm deep in the centrifuged pellet of cells.

Fig. 7 Axial scan through a 1.33/1.51 index mismatch with and without overlying cells. The data have been normalized to the peak signal value.

[Figure 6(b)]. The cell scattering in Figure 6(a) reduced the signal from the grating by a factor of 10. Assuming the attenuation of cell scattering follows Beer's Law, the optical thickness of the cells over the grating is 1.2 optical depths. The image of the grating is badly distorted by the overlying cells. The signal from the grating is lost in some places, indicating that the depth of focus has been moved off the plane of the grating. In other places, what should be a straight edge is curved. An image of the same grating is shown in Figure 6(b) under two optical depths of scattering from a suspension of 1 μm diameter polystyrene spheres. Very little, if any, distortion is observed with the polystyrene spheres. Due to the distortion caused by the cells, it is not possible to quantify the lateral resolution in Figure 6(a).

The effect of cellular scattering on the microscope's axial resolution was measured from the peak at the junction between the cell solution and a microscope slide. A typical scan from the 1.33/1.51 index mismatch is plotted in Figure 7 with and without overlying cells. The FWHM of the signal peak in Figure 7 increased from 2 μm without cells to 4.5 μm with the addition of the cells. The small peaks from individual cells to the left of the glass surface indicate that the cell layer was approximately 45 μm thick. The average FWHM axial resolution from ten locations was 3.9$\pm$2.4 μm with the addition of cells.

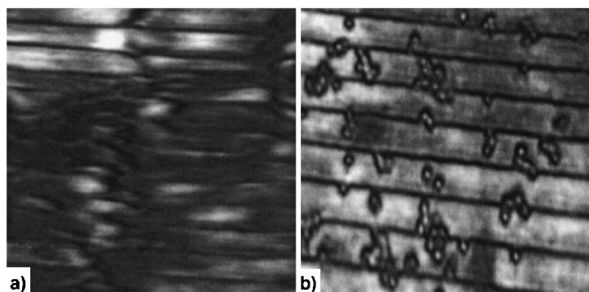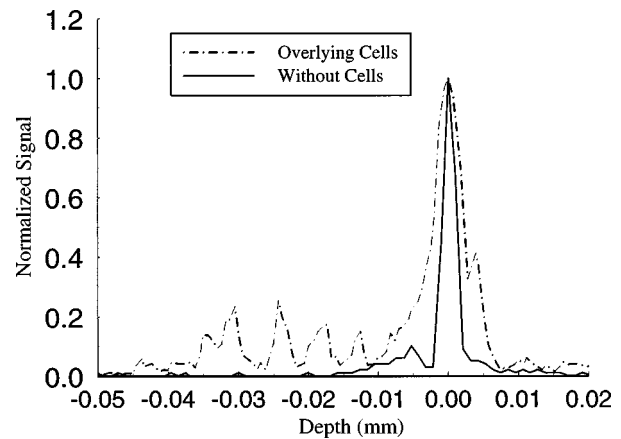To evaluate a potential method to increase the contrast in the confocal images, we imaged the breast cancer cells before [Figure 8(a)] and after exposure to acetic acid [Figure 8(b)]. In the images of native cells, the nuclei and cell membranes are resolvable; however, the contrast varies from cell to cell. The addition of acetic acid to the native cells causes a dramatic increase in the signal from the nuclei and the intracellular contents resulting in increased image contrast. The presence of a dark band surrounding the nuclei is apparent after adding the acetic acid. This is consistent with changes in the index profile noted with phase contrast microscopy. Figure 8 shows phase contrast images of these cells pre- [Figure 8(d)] and post- [Figure 8(e)] exposure to acetic acid. The addition of acetic acid results in increased fluctuations in the nuclear index of refraction and increased index difference between the nucleus and cytoplasm. ALA was also evaluated as a contrast agent. Figure 8(c) shows the effects of ALA on the native cells. In this case, the signal from the entire cell increased. However, the contrast between the nucleus and the cytoplasm is diminished. The same illumination power was used for all of the images in Figure 8.

4 DISCUSSION

It is apparent from Figures 3(a), 5(a), and 8 that confocal reflectance imaging has the potential to image cellular structure in amelanotic epithelial cells. The chromatin within the nucleus provides the strongest signal in the breast cancer cells, allowing the user to resolve the outline of the nucleus and some information about the structure within such as the nucleolus and the density of chromatin material. The observed nuclear contrast might be used to assess the pathological measures of nuclear shape and texture. In general, the amount of signal from the intracellular bodies is less than that from the nucleus. In the absence of distinct signal from the cell membranes, it is not possible to discern one cell's cytoplasm from that of adjacent cells when the cells are bound together. This is consistent with
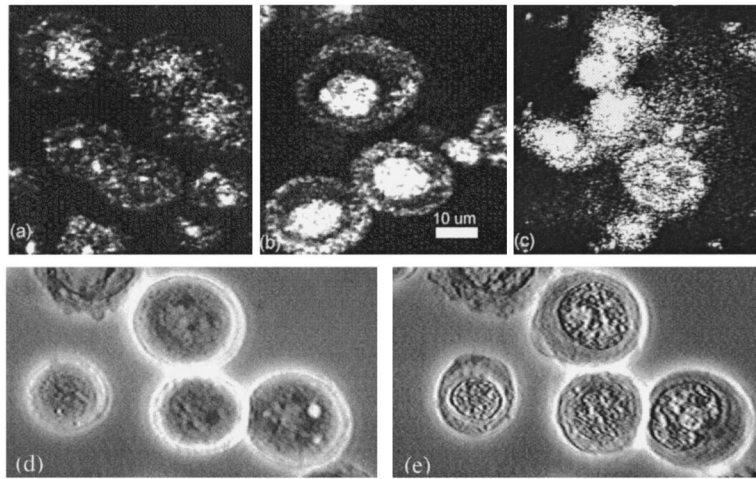

Fig. 6 300 lines/mm grating under (a) multiple layers of cells and (b) two optical depths of scattering from 1 μm polystyrene spheres.

Fig. 8 Confocal images of breast cancer cells in (a) saline, (b) saline after the addition of 6% acetic acid, and (c) in saline after the addition of 2% ALA. Phase contrast images of breast cancer cells in (d) saline and (e) after the addition of 6% acetic acid.

the observations from Figure 5(b). As such, it will be necessary to measure the ratio of nuclear diameter to internuclear spacing rather than the typical measure of nuclear to cytoplasm ratio. The correspondence between the two measures has already been demonstrated for *in vivo* imaging of human epidermis.[7] Additionally, it should be pointed out that there may be important diagnostic information in the orientation of cells with respect to each other, since loss of organization occurs during neoplastic progression. In cell suspensions, this information is lost since cell orientations vary randomly.

It is important to understand the physiological source of contrast in confocal imaging in order to develop the diagnostic potential of this technology. Monte Carlo predictions that refractive index changes are a primary source of contrast in confocal imaging are supported by the correspondence between images obtained though phase contrast microscopy, in which intensity is related to refractive index,[17] and confocal microscopy. Both confocal and phase images demonstrate that the appearance of a cell is altered by the addition of acetic acid. It is hypothesized that acetic acid causes crosslinking between proteins in the nucleus, altering nuclear structure. Phase contrast images of cells after the addition of acetic acid display increased index fluctuations in the nucleus [Figure 8(d)]. The increased variations in refractive index result in more scattering, giving the nucleus a brighter appearance when viewed with a confocal microscope. The confocal images of the cells before and after acetic acid demonstrate the sensitivity of confocal imaging to changes in cellular biochemical and morphologic composition. In addition, the images suggest it is possible to develop methods to enhance contrast of diagnostically valuable subcellular structure.

The results also demonstrate several mechanisms by which the contrast available to confocal imaging can be degraded. Contrast loss to interference effects will be dependent upon the geometry of imaged cells. The geometry of the average red blood cell[18] is shown in the inset to Figure 4(a) to illustrate the origin of the observed interference. When the focal plane is located in the center of the blood cell, both faces of the cell membrane are within the 2 μm axial resolution of the microscope and both contribute signal. Light reflected from both faces is incident at the detector and depending on the separation between the faces, interferes constructively or destructively. Based upon the average dimensions of the red blood cell, approximately three to four interference fringes should be observed between the center and edge of the cell. This is consistent with the number of fringes in Figure 4(a). The same rationale explains the fringes observed at the edges of the algae cells in Figure 4(b). At the edge of the cell, both faces of the plant cell wall are within the focal volume resulting in interference between them. In the interior of the cell, the separation between interfaces is greater than the axial resolution and no interference is observed. Interference effects will occur any time two or more reflective structures occupy the focal volume ($\sim$1 μm $\times$1 μm$\times$2 μm) at the same time.

Figures 6(a) and 7 illustrate that the refraction of overlying cells can distort and degrade the resolution of confocal images. It is important to note that the scattering of 1.0 μm diameter polystyrene microspheres does not produce this same effect; although the scattering coefficient is greater than that of the cells, the phase functions are sufficiently different to yield dramatically different results for high-resolution imaging. To further investigate the beam distortion caused by scattering in the overlying layers, a model of light propagation through inhomogeneous media was used. The model is based on the FDTD method, which is a numerical solution to Maxwell's equations for inhomogeneous
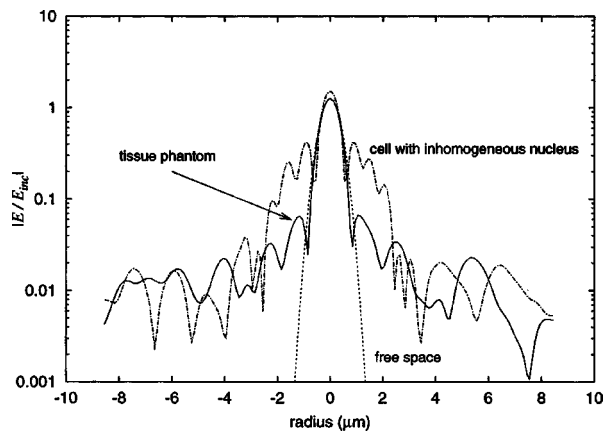
Fig. 9 Field distribution of a focused Gaussian beam in the FDTD model after propagating through a cell or a polystyrene sphere tissue phantom.

media. In the FDTD approach, the scattering object is discretized on a three dimensional lattice whose maximum grid spacing is $\lambda/10$. The electric and magnetic fields at each point in the lattice are computed as the incident field is propagated through the lattice. The details of the FDTD simulation can be found in Ref. 19. Due to computational limitations arising from the fine discretization, the model is limited to a volume of approximately 15 μm/side. To illustrate the observed differences in resolution degradation resulting from the polystyrene based phantom and the overlying cells, two situations were modeled. In the first case, a cell containing an inhomogeneous nucleus as well as cytoplasmic organelles was considered and in the second case a volume of gelatin containing 1 μm diameter polystyrene spheres was used with a volume number density equal to that of the phantom used in the experiments described previously. A focused Gaussian beam (NA=0.8) was propagated through both the cell and the phantom and the steady state fields throughout each volume were computed. The beam profile at its focus, transverse to the direction of propagation, is plotted in Figure 9 for the cell and the phantom. While there was little difference in the FWHM values of the beam profiles, the cell causes considerably more beam spreading than the tissue phantom, where the side lobes are significantly greater for the beam passing though a cell than a phantom.

Since resolution is dependent upon the point spread function of the focused beam, Figure 9 indicates that the resolution of an object located below a layer of cells will differ from that of an object below polystyrene based tissue phantom. In the case of propagation through a cell, the wave encounters a spatially dependent refractive index profile that varies continuously throughout the cell. The magnitude of the refractive index fluctuations is small compared to the index mismatch between a polystyrene sphere and gelatin. However, the number of spheres per volume ($5.5 \times 10^6/\text{mm}^3$) is small so

that the average spacing between spheres is large compared to the scale of the index fluctuations in cells. The fundamental difference between these scattering mechanisms demonstrates that polystyrene spheres may not be an appropriate model to study the effects of tissue scattering on high-resolution confocal reflectance imaging.

To understand some of the difficulty of *in vivo* imaging, it is necessary to consider the impact of distortion and resolution degradation on cellular imaging. The images of the grating under the cells overemphasize the effects of the distortion on cellular imaging. The confocal signal from the grating is lost if the focus is axially displaced by a few microns. If the focus is laterally displaced by a few microns, the lines appear to run into each other. The axial resolution measurements indicate that axial displacements up to 5 μm were observed. For cellular imaging, the signal will not be lost if the focus is displaced by a few microns. Instead, the signal from adjacent structure will be included in the sample. Considering that epithelial nuclei are 5–10 μm in diameter and are separated by 10–20 μm, it is expected that any detail within the nuclei will be washed out but the signal from adjacent nuclei will be distinct. This conclusion corresponds well with observations in Figure 5(b). The other significant effect of the distortion is the displacement of the nuclei boundaries in the image plane. The impact of distorting the shape of the nuclei by a few microns in any direction is unclear at this point and should be addressed in future work.

The magnitude of the cell distortion is overestimated by the experiments with the cells suspended in saline. Cells in the native epithelium will be bound together, so that a photon traversing the cells would be incident on a cell membrane, the cytoplasm, possibly a nucleus, and then on to the next cell. Suspending the cells in saline adds at least two additional index mismatches to that path by separating the membranes and placing saline between them. The refractive index of the cytoplasm is approximately 1.37 and the index of the lipid cell membrane is approximately 1.45.[20] Adding the saline with an index of 1.33 will increase the amount of refraction occurring at the cell membranes as well as the number of mismatches. Barer[21] has demonstrated that changing the index of the suspension medium can have a significant effect on the scattering of cells. As such, these experiments represent a worst case scenario for the effects of cell scattering.

Although loss of resolution and contrast degradation will be a concern in *in vivo* confocal imaging regardless of the particular optical system employed (tandem light path, scanning slit, spinning disk, etc.), the numerical data presented in this work are most relevant to confocal instruments of similar design to the microscope used in this study. Signal to noise (S/N) and signal to background (S/B) ratios can vary significantly for instruments with different optical pathways.[22] For instance,

both S/B and S/N are much higher in our confocal microscope than in a spinning disk or slit detection system. The acceptable levels of degradation, which will still allow diagnostically useful imaging, will depend on numerous parameters concerning a particular system's optical design.

Figure 8(a) illustrates the potential improvement in image contrast with the application of acetic acid. Although the mechanism of the enhancement is unclear, acetic acid is apparently increasing the refractive index variations within cells. Previous work[9] predicts the penetration depth in ideal confocal systems is limited by the signal to noise ratio (S/N). In a S/N limited confocal microscope, the additional signal created by acetic acid would extend the maximum penetration depth. Pertinent questions which should be addressed in future work are the viability of cells after exposure to acetic acid and the ability of acetic acid to diffuse to subsurface layers of cells.

5 CONCLUSIONS

Contrast in confocal images of amelanotic cells is derived from index variations. In the breast cancer cells used for this study, the majority of signal arose from chromatin material in the nucleus. Confocal imaging of reflected light does have the potential to provide clinical indicators of cell pathology including the equivalent of N/C ratios, nuclear shape and texture. However, this work also demonstrates the difficulty in achieving the potential contrast due to scattering of the light in overlying layers. More work is needed to characterize the resolution losses from overlying cell scattering, however, the worst case portrayed here is a reduction in information to a N/C volume ratio estimate. The application of acetic acid shows potential for increasing confocal contrast over that of native cells. Unlike most previous work in which images are obtained in real time but then enhanced via time intensive image processing techniques, we present images as they appear at the time of acquisition without any post-processing. These images are representative of what would be possible for clinical applications requiring near video rate imaging and demonstrate the promise of this emerging technology for aiding standard histopathologic diagnosis.

Acknowledgments

REFERENCES

1. *Handbook of Biological Confocal Microscopy*, J. Pawley, Ed., 2nd ed., Plenum, New York (1995).
2. J. V. Jester, P. M. Andrews, W. M. Petroll, M. A. Lemp, and H. D. Cavanaugh, ''In vivo, real-time confocal imaging,'' *J. Electron Microsc. Tech.* **18**, 50–60 (1991).
3. J. V. Jester, W. M. Petroll, R. M. Garana, M. A. Lemp, and H. D. Cavanaugh, ''Comparison of *in vivo* and *ex vivo* cellular structure in rabbit eyes detected by tandem scanning microscopy,'' *J. Microsc.* **165**, 169–181 (1992).
4. B. Masters and A. A. Thaer, ''Real-time scanning slit confocal microscopy of the *in vivo* human cornea,'' *Appl. Opt.* **33**, 695–701 (1994).
5. C. Bertrand and P. Corcuff, ''In vivo spatio-temporal visualization of the human skin by real-time confocal microscopy,'' *Scanning* **16**, 150–154 (1994).
6. P. Corcuff, G. Gonnord, G. E. Pierard, and J. L. Leveque, ''*In vivo* microscopy of human skin: A new design for cosmetology and dermatology,'' *Scanning* **18**, 351–355 (1996).
7. Rajadhyaksha, M. Grossman, D. Esterowitz, R. H. Webb, and R. R. Anderson, ''*In vivo* confocal scanning laser microscopy of human skin: Melanin provides strong contrast,'' *J. Invest. Dermatol.* **104**, 946–952 (1995).
8. B. R. Masters, D. J. Aziz, A. F. Gmitro, J. H. Kerr, T. C. O'Grady, and L. Goldman, ''Rapid observation of unfixed, unstained human skin biopsy specimens with confocal microscopy and visualization,'' *J. Biomed. Opt.* **2**, 437–445 (1998).
9. C. L. Smithpeter, A. K. Dunn, A. J. Welch, and R. Richards-Kortum, ''Penetration depth limits of *in vivo* confocal reflectance imaging,'' *Appl. Opt.* **37**, 2749–2754 (1998).
10. A. K. Dunn, C. Smithpeter, A. Welch, and R. Richards-Kortum, ''Sources of contrast in confocal reflectance imaging,'' *Appl. Opt.* **35**, 3441–3446 (1996).
11. T. Wilson, ''The role of the pinhole in confocal imaging systems,'' in *Handbook of Biological Confocal Microscopy*, J. Pawley, Ed., pp. 99–113, Plenum, New York (1995).
12. P. C. Cheng and A. Kriete, ''Image contrast in confocal light microscopy,'' in *Handbook of Biological Confocal Microscopy*, J. Pawley, Ed., pp. 281–310, Plenum, New York (1995).
13. R. Juskaitis, T. Wilson, and T. F. Watson, ''Real-time white light reflection confocal microscopy using a fiber-optic bundle,'' *Scanning* **19**(1), 15–19 (1997).
14. A. Leung et al., ''Fluorescence imaging and spectroscopy of 5-aminolevulinic acid induced protoporphyrin IX for the detection of neoplastic lesions in the oral cavity,'' *Am. J. Surg.* **172**, 674–677 (1996).
15. L. Ozzello, *The Breast*, Williams and Wilkins, Baltimore (1984).
16. M. Kempe, W. Rudolph, and E. Welsch, ''Comparative study of confocal and heterodyne microscopy for imaging through scattering media,'' *J. Opt. Soc. Am. A* **13**, 46–52 (1996).
17. F. Beltrame, B. Bianco, and A. Chiabrera, ''Automated analysis of living cells through the quantitative use of automated phase contrast microscopy,'' *Cell Biophys.* **6**, 103–115 (1984).
18. Elaine Marieb, *Human Anatomy and Physiology*, 2nd ed., Benjamin/Cummings, Redwood City, CA (1992).
19. A. Dunn and R. Richards-Kortum, ''3-dimensional computation of light-scattering from cells,'' *IEEE J. Sel. Top. Quantum Electron.* **2**(4), 898–905 (1996).
20. A. Brunsting and P. Mullaney, ''Differential light scattering from spherical mammalian cells,'' *Biophys. J.* **14**, 439–453 (1974).
21. R. Barer, ''Refractometry and interferometry of living cells,'' *J. Opt. Soc. Am.* **47**, 545–556 (1956).
22. D. R. Sandison and W. W. Webb, ''Background rejection and signal to noise ratio optimization in confocal and alternative fluorescence microscopes,'' *Appl. Opt.* **33**, 603–615 (1994).